EnMAP Hyperspectral Imager

EnMAP Technical Report

2013 Simulated EnMAP Mosaics for the San Francisco Bay Area, USA

Sam Cooper, Akpona Okujeni, Clemens Jänicke,
Karl Segl, Sebastian van der Linden, Patrick Hostert

Recommended citation of the report:

Cooper, S., Okujeni, A., Jänicke, C., Segl, K., van der Linden, S., Hostert, P., (2020), 2013 Simulated EnMAP Mosaics for the San Francisco Bay Area, USA. EnMAP Technical Report, GFZ Data Services.
DOI: https://doi.org/10.2312/enmap.2020.002

Supplementary datasets:

Cooper, S., Okujeni, A., Jänicke, C., Segl, K., van der Linden, S., Hostert, P., (2020), 2013 Simulated EnMAP Mosaics for the San Francisco Bay Area, USA, GFZ Data Services.
DOI https://doi.org/10.5880/EnMAP.2020.002

Key publication:

Cooper, S., Okujeni, A., Jänicke, C., Clark, M., & van der Linden, S., Hostert, P. (2020). Disentangling fractional vegetation cover: regression-based unmixing of simulated spaceborne imaging spectroscopy data. Remote Sensing of Environment, 246, 111856.
DOI https://doi.org/10.1016/j.rse.2020.111856

Imprint

EnMAP Consortium

Helmholtz Centre Potsdam
GFZ German Research Centre for Geosciences

Publisher
GFZ Data Services

Telegrafenberg
D-14473 Potsdam
2020

DOI: https://doi.org/10.2312/enmap.2020.002

EnMAP

Technical Report

2013 Simulated EnMAP Mosaics for the San Francisco Bay Area, USA

Sam Cooper[1], Akpona Okujeni[1], Clemens Jänicke[1], Karl Segl[2], Sebastian van der Linden[3], Patrick Hostert[1]

[1] *Humboldt-Universität zu Berlin, Berlin, Germany*

[2] *GFZ German Research Centre for Geosciences, Potsdam, Germany*

[3] *Universität Greifswald, Greifswald, Germany*

Supported by:

Federal Ministry for Economic Affairs and Energy

on the basis of a decision by the German Bundestag

Table of Contents

1. Abstract

This dataset is composed of simulated EnMAP mosaics for the San Francisco Bay Area, USA. Hyperspectral imagery used for the EnMAP simulation was collected across three time periods (Spring, Summer, and Fall) in 2013 with the AVIRIS-Classic sensor flown as part of the HyspIRI Preparatory Campaign. Flight lines were simulated to EnMAP-like data using the EnMAP end-to end Simulation tool to produce 30 x 30 m imagery with 195 bands (after band removal) ranging from 423 to 2439 nm. Secondary geometric correction was applied using automatically generated tie points, and a class-wise empirical across track brightness correction was implemented to mitigate brightness gradients.

Coordinates:	**Centroid:**	37.91 N / 122.16 W
	NW:	39.06 N / 123.52 W
	NE:	39.06 N / 120.76 W
	SE:	36.38 N / 120.76 W
	SW:	36.38 N / 123.52 W

Keywords: Hyperspectral Imagery, EnMAP, AVIRIS, California, Vegetation

Related sources:

An overview of the EnMAP mission is provided in Guanter et al. (2015):

> Guanter, L., Kaufmann, H., Segl, K., Foerster, S., Rogaß, C., Chabrillat, S., …, and Sang, B. (2015). The EnMAP spaceborne imaging spectroscopy mission for earth observation. *Remote Sensing*, 7(7), 8830-8857. https://doi.org/10.3390/rs70708830

A full description of the EnMAP end-to-end simulation tool is described in Segl et al. (2012):

> Segl, K., Guanter, L., Rogass, C., Kuester, T., Roessner, S., Kaufmann, H., Sang, B., Mogulsky, V., & Hofer, S. (2012). EeteS—The EnMAP end-to-end simulation tool. *IEEE Journal of Selected Topics in Applied Earth Observations and Remote Sensing*, 5, 522-530. https://doi.org/10.1109/JSTARS.2012.2188994

An in-depth test of the across track brightness correction method used for this data is presented by Jänicke et al., (2020):

> Jänicke, C., Okujeni, A., Cooper, S., Clark, M., Hostert, P., & van der Linden, S. (2020). Brightness gradient-corrected hyperspectral image mosaics for fractional vegetation cover mapping in northern California. *Remote Sensing Letters*, 11(1), 1-10. https://doi.org/10.1080/2150704X.2019.1670518

A companion study mapping fractional vegetation cover types is presented in Cooper et al., (in press):

> Cooper, S., Okujeni, A., Jänicke, C., Clark, M., & van der Linden, S., Hostert, P. (2020). Disentangling fractional vegetation cover: regression-based unmixing of simulated spaceborne imaging spectroscopy data. *Remote Sensing of Environment*, 246, 111856. https://doi.org/10.1016/j.rse.2020.111856

1 Introduction

The Environmental Mapping and Analysis Program (EnMAP) is a German hyperspectral satellite mission that aims at monitoring and characterizing the Earth's environment on a global scale (Guanter et al., 2015). EnMAP serves to measure and model key dynamic processes of the Earth's ecosystems by extracting geochemical, biochemical and biophysical parameters, which provide information on the status and evolution of various terrestrial and aquatic ecosystems. In the frame of the EnMAP preparatory phase, pre-flight campaigns including airborne and in-situ measurements in different environments and for several application fields are being conducted. The main purpose of these campaigns is to support the development of scientific applications for EnMAP. In addition, the acquired data are input in the EnMAP end-to-end simulation tool (EeteS) and are employed to test data pre-processing and calibration-validation methods. The campaign data are made freely available to the scientific community under a Creative Commons Attribution 4.0 International License (CC BY-4.0). An overview of all available data is provided in a specifically developed metadata portal on the project website (http://www.enmap.org/?q=flights).

This dataset is centered on the San Francisco Bay Area in Northern California, USA. The data is derived from Airborne Visible/Infrared Imaging Spectrometer (AVIRIS) classic imagery and was acquired as part of the HyspIRI preparatory Science campaign (Lee et al., 2015). AVIRIS reflectance images were simulated to approximate spaceborne EnMAP imagery, and class-wise across track brightness corrections as well as secondary geometric corrections were applied to the imagery. Included with the image data is an image based spectral library derived from the summer image as well as reference fractional cover classes developed and described in Cooper et al. (in rev). This is a ready-to-use dataset for regional scale hyperspectral unmixing demonstrating the capabilities of forthcoming spaceborne imaging spectroscopy data.

The study area covers approximately 30,000 km^2 in a predominantly Mediterranean climate. Water availability varies with precipitation patterns, topography, and underlying soils, and is a key driver of vegetation composition, structure and function both at a micro and landscape scale. This leads to a complex mosaic of vegetation types locally, and a transition of vegetation communities from a more temperate climate along the coast to a more arid climate in the east and south. Dense urban areas dominate the region immediately around the San Francisco Bay, with smaller cities and towns interspersed around the study area. The Central Valley in the east of the study region is predominantly composed of agricultural lands, with intensive agriculture also present in the valleys north of the bay.

2 Data Acquisition

Orthorectified AVIRIS reflectance images were obtained from the JPL AVIRIS data portal (http://aviris.jpl.nasa.gov). The AVIRIS pre-processing chain implemented by the Jet Propulsion Laboratory (JPL) consists of radiometric correction, orthorectification, and atmospheric correction using a modified version of the ATmospheric REMoval program (ATREM; Thompson et al., 2015).

The AVIRIS is a NASA Earth Science airborne sensor developed by JPL, and for the HyspIRI preparatory Science campaign the sensor was flown aboard the ER-2 at altitude of approximately 20 km. Flight lines were on average 240 km long with a swath width of approximately 12 km. Overlap between adjacent flight lines was approximately 20% with a maximum view angle of ±17°. The imagery had 224 bands between 400 and 2500 nm.

Three acquisition periods were used in 2013 (Table 1), roughly corresponding to different stages in plant phenological cycles. For simplicity these three acquisitions are referred to here as spring, summer and fall. Due to cloudy conditions, three different acquisition dates were used in the fall campaign. Details of the individual flight lines can be found in appendices 9.1, 9.2, and 9.3.

Table 1: AVIRIS acquisition times

Campaign	Date	UTM Start	UTM Stop	Avg. pixel size (m)
Spring	April 10th, 2013	17:52	22:23	16.3
Summer	June 7th, 2013	18:37	23:21	16.5
Fall 1	November 22th, 2013	18:13	20:44	16.4
Fall 2	December 4th, 2013	20:17	21:17	16.3
Fall 3	December 5th, 2013	19:01	21:22	16.1

3 Data Processing and Products

Each AVIRIS reflectance image was converted into a 30 m EnMAP scene using the EnMAP end-to-end simulator (EeteS; Segl et al., 2012). In total 242 EnMAP bands were simulated from the AVIRIS imagery using the EeteS. Bands near strong atmospheric water absorption regions (1,311 – 1,465 nm and 1,783 – 2,044 nm) were removed, as were five bands in the NIR (934-952 nm) with poor reflectance retrievals. After band removal, 195 simulated EnMAP bands remained.

Across track brightness gradient correction was conducted to remove brightness gradients originating from the varying sun-sensor geometries between flight lines. A class-wise empirical across-track brightness correction approach following Schiefer et al. (2006) was implemented and describe in detail in Jänicke et al. (2020). In short, images were classified into three classes roughly corresponded to green vegetation, non-photosynthetically active vegetation (NPV) and non-vegetation. A band-wise correction factor was generated by fitting a quadratic model to each band across the range of view angles for each vegetation strata, and nadir normalized values were created by dividing the reflectance of a given pixel by the correction factor derived from the pixel's class and across-track location. The non-vegetation class, corresponding to water and urban areas were corrected with the NPV class.

While initial orthorectification was carried out by JPL, georeferencing errors were still observed in the imagery. A secondary geometric correction was therefore applied to each flight line by co-registering the simulated EnMAP flight lines to contemporaneous Landsat imagery. Tie points were automatically generated using the Automated and Robust Open-Source Image Co-Registration Software (AROSICS; Scheffler et al., 2017). Estimated local shifts ranged from less than 3 m to greater than 150 m. The EnMAP imagery was corrected using these tie points with a third-degree polynomial and bilinear resampling, and remaining residual shifts were observed only at subpixel levels.

The corrected images were then mosaicked into a single image, with western flight lines overlaying eastern flight lines. The final data configuration of the EnMAP simulations are described in Table 2.

Table 2: Simulated EnMAP data description

Simulated EnMAP Data Description	
Units	Surface Reflectance (*10,000)
Geometric Resolution	30 m x 30 m
Spectral Bands	195
Spectral Range	423 – 2439 nm
Spectral Sampling Distance	6.5 nm (VNIR) 10 nm (SWIR)
Projection	UTM 10N EPSG: 32610

4 File Description

4.1 File Format

Band Sequential Image File [*.bsq] and file header [*.hdr]

4.2 Data content and structure

To facilitate data storage and access, the simulated EnMAP mosaics have been subdivided into two subset regions (Figure 1). The northern region is 7000 x 5000 pixels (210 x 150 km) and the southern region is 6000 x 5000 pixels (180 x 150 km).

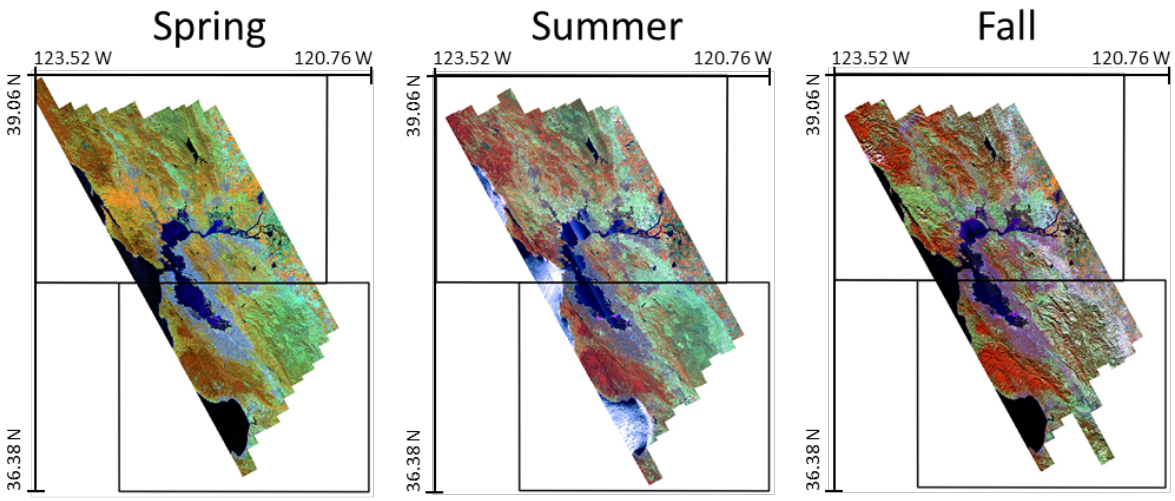

Figure 1: EnMap mosaics for the San Francisco Bay Area, USA displaying the Spring, Summer, and Fall 2013 EnMAP mosaics with the northern and southern subset boxes

All image files from a given EnMAP scene share a common prefix with the following form:

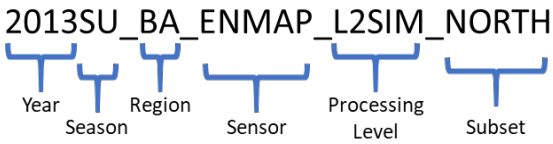

Year (2013) and Season (SP: Spring, SU: Summer, FA: Fall) indicate the acquisition timeframe. Region (BA: SF Bay Area), indicates the region in the context of the HyspIRI Preparatory Flight Campaign. The processing level represents the in-house processing stage, were L2 indicates it is a reflectance image with secondary geometric and brightness corrections applied to the imagery and SIM indicates it is a simulated dataset of the listed sensor. The subset indicates the image is from either the NORTH or SOUTH subset.

Image files are described in the header file by the following attributes:
ENVI description, samples, lines, bands, header offset, file type, data type, interleave, byte order, map info, coordinate system string, wavelength units, band names, wavelength, full width half maximum (fwhm)

5 Additional Data

5.1 Image-based Spectral Library

An image-based spectral library developed in Cooper et al. (in rev) is available for download ("BA_SpectralLibrary_su2013.sli"). Table 3 describes the associated metadata files.

Table 3: Spectral library file components

File Type	Extension	Description
ENVI Spectral Library	*.sli	ENVI spectral profiles
ENVI Header	*.hdr	ENVI metadata file describing spectral properties
Comma Separated	*.csv	Metadata file containing spectra names and labels
JSON	*.json	Metadata file for integration into the EnMAP box

A total of 1,841 pure spectra were collected throughout the study area. High resolution Google Earth imagery was used to identify areas of homogenous vegetation cover at the maximum density observed in the study region. Delineated homogenous areas ranged from 1 to 10 EnMAP pixels, and the mean spectrum was extracted from each area. Spectra in the library consist of a unique spectra name to link the spectra to relevant metadata.

Vegetation classes used in the library were created in a hierarchical manner, with spectra collected at Level 4 (Table 4). Higher level classes were created by combining spectra from the appropriate lower levels. These levels are defined as separate classification schemes in the .csv and .json files of the spectral library.

Table 4: Vegetation classes in the spectral library

Level 1	Vegetation				Non-Vegetation
Level 2	Woody Vegetation			Non-woody Vegetation	Non-Vegetation
Level 3	Trees		Shrubs	Non-woody Vegetation	Non-Vegetation
Level 4	Needleleaf	Broadleaf	Shrubs	Non-woody Vegetation	Non-Vegetation

5.2 Vegetation Fractional Cover References

A vector file containing fractional cover estimates for vegetation classes corresponding to the spectral library (5.2) is also available for download as a shapefile ("BA_VegFractions_su2013.shp"). This dataset was developed in Cooper et al. (in rev). 241 validation sites were randomly selected within pre-defined areas representing typical 'natural' vegetation (i.e. urban and agricultural areas were excluded from the reference data). An additional 14 validation sites were selected to better represent non-vegetation in the validation dataset. The total number of validation polygons is 255.

Each polygon consists of a 3x3 pixel block at each validation site, and Level 4 class fractions for each pixel in the polygons were estimated independently by two experts through visual interpretation of high-resolution Google Earth imagery. The two independent estimates were then averaged, and discrepancies greater than 25% between the two estimates were reviewed and appropriate fractions were agreed upon. The polygon attributes consist of unique polygon IDs as well as Level 4 estimates and unique higher-level classes (i.e. Vegetation, Woody Vegetation, and Trees).

6 Dataset Contact

Sam Cooper
Email: sam.cooper@geo.hu-berlin.de

Akpona Okujeni
Email: akpona.okujeni@geo.hu-berlin.de

Sebastian van der Linden
Email: sebastian.linden@uni-greifswald.de

7 Acknowledgements

We would like to thank NASA Jet Propulsion Laboratory (JPL) for providing AVIRIS imagery. The simulated EnMAP mosaic was generated as part of the EnMAP Core Science Team activities funded by the German Aerospace Centre (DLR) Space Administration and granted by the Ministry of Economics and Energy (BMWi; grant number 50EE1622).

8 References

Cooper, S., Okujeni, A., Jänicke, C., Clark, M., & van der Linden, S., Hostert, P. 2020). Disentangling fractional vegetation cover: regression-based unmixing of simulated spaceborne imaging spectroscopy data. Remote Sensing of Environment, 246, 111856. https://doi.org/10.1016/j.rse.2020.111856

Guanter, L., Kaufmann, H., Segl, K., Foerster, S., Rogaß, C., Chabrillat, S., Küster, T., Hollstein, A., Rossner, G., Chlebek, C., Straif, C., Fischer, S., Schrader, S., Storch, T., Heiden, U., Mueller, A., Bachmann, M., Mühle, H., Müller, R., Habermeyer, M., Ohndorf, A., Hill, J., Buddenbaum, H., Hostert, P., van der Linden, S., Leitão, P., Rabe, A., Doerffer, R., Krasemann, H., Xi, H., Mauser, W., Hank, T., Locherer, M., Rast, M., Staenz, K., Sang, B. (2015). The EnMAP spaceborne imaging spectroscopy mission for earth observation. *Remote Sensing*, 7(7), 8830-8857. https://doi.org/10.3390/rs70708830

Jänicke, C., Okujeni, A., Cooper, S., Clark, M., Hostert, P., & van der Linden, S. (2020). Brightness gradient corrected hyperspectral image mosaics for mapping vegetation cover fractions in the San Francisco Bay Area. *Remote Sensing Letters*. 11(1), 1-10. https://doi.org/10.1080/2150704X.2019.1670518

Lee, C.M., Cable, M.L., Hook, S.J., Green, R.O., Ustin, S.L., Mandl, D.J., & Middleton, E.M. (2015). An introduction to the NASA Hyperspectral InfraRed Imager (HyspIRI) mission and preparatory activities. *Remote Sensing of Environment*, 167, 6-19. https://doi.org/10.1016/j.rse.2015.06.012

Scheffler, D., Hollstein, A., Diedrich, H., Segl, K., & Hostert, P. (2017). AROSICS: An automated and robust open-source image co-registration software for multi-sensor satellite data. *Remote Sensing*, 9, 676. https://doi.org/10.3390/rs9070676

Schiefer, S., Hostert, P., & Damm, A. (2006). Correcting brightness gradients in hyperspectral data from urban areas. *Remote Sensing of Environment*, 101(1), 25-37. https://doi.org/10.1016/j.rse.2005.12.003

Segl, K., Guanter, L., Rogass, C., Kuester, T., Roessner, S., Kaufmann, H., Sang, B., Mogulsky, V., & Hofer, S. (2012). EeteS—The EnMAP end-to-end simulation tool. *IEEE Journal of Selected Topics in Applied Earth Observations and Remote Sensing*, 5, 522-530. http://doi.org/10.1109/JSTARS.2012.2188994

Thompson, D.R., Gao, B.C., Green, R.O., Roberts, D.A., Dennison, P.E., & Lundeen, S.R. (2015). Atmospheric correction for global mapping spectroscopy: ATREM advances for the HyspIRI preparatory campaign. *Remote Sensing of Environment*, 167, 64-77. https://doi.org/10.1016/j.rse.2015.02.010

9 Appendices

9.1 Spring Campaign

Site Name	AVIRIS Flight Name	Start Lat	Start Lon	Stop Lat	Stop Lon	Start GMT	Stop GMT
BA49	f130410t01p00r11	36.54517794	-121.8265158	38.87996861	-123.4353324	1819	1850
BA50	f130410t01p00r10	36.58864431	-121.725596	38.92343497	-123.3311763	1752	1816
BA51	f130410t01p00r12	36.63168581	-121.625344	38.96647648	-123.2277042	1853	1916
BA52	f130410t01p00r13	36.67463986	-121.5249778	39.00943053	-123.1241091	1921	1945
BA53	f130410t01p00r15	36.71750622	-121.4244973	39.05229688	-123.020391	2012	2034
BA54	f130410t01p00r14	36.76028465	-121.3239025	39.09507532	-122.9165499	1947	2007
BA55	f130410t01p00r16	36.80264142	-121.2239804	39.13743209	-122.8133982	2036	2056
BA56	f130410t01p00r17	36.84457835	-121.1247338	39.17936902	-122.7109389	2100	2120
BA57	f130410t01p00r19	36.88642942	-121.0253762	39.22122009	-122.6083601	2143	2203
BA58	f130410t01p00r18	36.9281944	-120.9259076	39.26298507	-122.5056617	2122	2139
BA59	f130410t01p00r20	36.97020387	-120.8255371	39.30499453	-122.4020272	2206	2223

Site Name	AVIRIS Flight Name	Pixel Size	Flight Angle from North	Solar Elevation	Solar Azimuth
BA49	f130410t01p00r11	16.4	-28	53.04	137.81
BA50	f130410t01p00r10	16.4	-29	48.72	128.09
BA51	f130410t01p00r12	16.4	-29	56.64	149.21
BA52	f130410t01p00r13	16.3	-29	59.04	162.2
BA53	f130410t01p00r15	16.2	-29	59.97	186.87
BA54	f130410t01p00r14	16.0	-29	59.95	174.16
BA55	f130410t01p00r16	16.0	-29	58.88	198.3
BA56	f130410t01p00r17	16.1	-29	56.9	209.02
BA57	f130410t01p00r19	16.2	-29	51.69	225.2
BA58	f130410t01p00r18	16.6	-29	54.58	217.18
BA59	f130410t01p00r20	16.8	-29	48.27	232.2

9.2 Summer Campaign

Site Name	AVIRIS Flight Name	Start Lat	Start Lon	Stop Lat	Stop Lon	Start GMT	Stop GMT
BA49	f130607t01p00r14	36.58864431	-121.725596	38.92343497	-123.3311763	2256	2321
BA50	f130607t01p00r13	36.54517794	-121.8265158	38.87996861	-123.4353324	2224	2249
BA51	f130607t01p00r12	36.63168581	-121.625344	38.96647648	-123.2277042	2156	2219
BA52	f130607t01p00r11	36.67463986	-121.5249778	39.00943053	-123.1241091	2129	2152
BA53	f130607t01p00r09	36.71750622	-121.4244973	39.05229688	-123.020391	2036	2059
BA54	f130607t01p00r10	36.76028465	-121.3239025	39.09507532	-122.9165499	2103	2124
BA55	f130607t01p00r08	36.80264142	-121.2239804	39.13743209	-122.8133982	2009	2030
BA56	f130607t01p00r07	36.84457835	-121.1247338	39.17936902	-122.7109389	1946	2005
BA57	f130607t01p00r05	36.88642942	-121.0253762	39.22122009	-122.6083601	1859	1918
BA58	f130607t01p00r06	36.9281944	-120.9259076	39.26298507	-122.5056617	1923	1941
BA59	f130607t01p00r04	36.97020387	-120.8255371	39.30499453	-122.4020272	1837	1854

Site Name	AVIRIS Flight Name	Pixel Size	Flight Angle from North	Solar Elevation	Solar Azimuth
BA49	f130607t01p00r14	16.5	-29	48.44	262.33
BA50	f130607t01p00r13	16.6	-29	54.6	255.79
BA51	f130607t01p00r12	16.7	-29	59.96	248.69
BA52	f130607t01p00r11	16.4	-29	64.85	239.8
BA53	f130607t01p00r09	16.3	-29	72.32	213.75
BA54	f130607t01p00r10	16.3	-29	68.85	229.14
BA55	f130607t01p00r08	16.2	-29	74.45	193.18
BA56	f130607t01p00r07	16.2	-29	74.59	171.78
BA57	f130607t01p00r05	16.5	-29	70.66	138.49
BA58	f130607t01p00r06	16.8	-29	73.25	153.96
BA59	f130607t01p00r04	16.9	-29	67.45	127.43

9.3 Fall Campaign

NOTE: flight dates are indicated in the AVIRIS flight name in the first six digits in the following format: YYMMDD.

Site Name	AVIRIS Flight Name	Start Lat	Start Lon	Stop Lat	Stop Lon	Start GMT	Stop GMT
BA49	f131205t01p00r07	36.54517794	-121.8265158	38.87996861	-123.4353324	1928	1953
BA50	f131205t01p00r06	36.58864431	-121.725596	38.92343497	-123.3311763	1901	1921
BA51	f131205t01p00r08	36.63168581	-121.625344	38.96647648	-123.2277042	1959	2018
BA52	f131122t01p00r12	38.844	-123.007	37.35	-12.967	2027	2044
BA52	f131205t01p00r10	36.67463986	-121.5249778	39.00943053	-123.1241091	2046	2053
BA53	f131122t01p00r11	37.433333	-121.85	38.84733	-122.87567	2005	2022
BA53	f131205t01p00r09	36.71750622	-121.4244973	39.05229688	-123.020391	2030	2039
BA54	f131122t01p00r10	38.8505	-122.744333	37.55	-121.85	1945	1800
BA54	f131205t01p00r11	36.76028465	-121.3239025	39.09507532	-122.9165499	2057	2108
BA55	f131122t01p00r09	37.6	-121.75	38.8531667	-122.613833	1925	1940
BA55	f131205t01p00r12	36.80264142	-121.2239804	39.13743209	-122.8133982	2115	2122
BA56	f131122t01p00r08	38.8555	-122.484	37.6667	-121.667	1906	1919
BA56	f131204t01p00r12	36.84457835	-121.1247338	39.17936902	-122.7109389	2031	2039
BA57	f131122t01p00r06	38.85767	-121.35433	37.667	-121.533	1828	1841
BA57	f131204t01p00r15	36.88642942	-121.0253762	39.22122009	-122.6083601	2109	2117
BA58	f131122t01p00r07	37.7	-121.533	38.8595	-122.2245	1848	1902
BA58	f131204t01p00r13	36.9281944	-120.9259076	39.26298507	-122.5056617	2045	2052
BA59	f131122t01p00r05	37.9	-121.4333	38.86167	-122.094	1813	1824
BA59	f131204t01p00r11	36.97020387	-120.8255371	39.30499453	-122.4020272	2017	2026

Site Name	AVIRIS Flight Name	Pixel Size	Flight Angle from North	Solar Elevation	Solar Azimuth
BA49	f131205t01p00r07	16.3	-29	29.77	174.42
BA50	f131205t01p00r06	16.3	-29	28.74	166.88
BA51	f131205t01p00r08	16.2	-29	29.78	182.31
BA52	f131122t01p00r12	16.6	-29	31.02	190.95
BA52	f131205t01p00r10	16.1	-29	29.16	193.72
BA53	f131122t01p00r11	16.1	-29	31.51	185.3
BA53	f131205t01p00r09	16.0	-29	29.93	189.51
BA54	f131122t01p00r10	15.9	-29	31.67	179.37
BA54	f131205t01p00r11	16.2	-29	28.27	197.49
BA55	f131122t01p00r09	16.2	-29	31.38	173.97
BA55	f131205t01p00r12	15.8	-29	27.14	201.25
BA56	f131122t01p00r08	16.3	-29	30.81	168.68
BA56	f131204t01p00r12	15.9	-29	29.54	190.23
BA57	f131122t01p00r06	16.3	-29	28.75	158.82
BA57	f131204t01p00r15	16.0	-29	27.53	200.1
BA58	f131122t01p00r07	16.7	-29	29.97	164.12
BA58	f131204t01p00r13	16.4	-29	28.91	193.84
BA59	f131122t01p00r05	16.7	-29	27.43	154.99
BA59	f131204t01p00r11	16.8	-29	29.69	187.04